ELSEVIER

NeuroImage

www.elsevier.com/locate/ynimg
NeuroImage 39 (2008) 1896–1909

Tonic and phasic electroencephalographic dynamics during continuous compensatory tracking

Ruey-Song Huang,[a,b,*] Tzyy-Ping Jung,[a,c] Arnaud Delorme,[a,d] and Scott Makeig[a]

[a]*Swartz Center for Computational Neuroscience, Institute for Neural Computation, University of California San Diego, La Jolla, CA 92093-0961, USA*
[b]*Department of Cognitive Science, University of California San Diego, La Jolla, CA 92093-0515, USA*
[c]*Brain Research Center, Department of Computer Science, National Chiao-Tung University, Hsinchu, 30010, Taiwan*
[d]*CerCo,Université Toulouse 3, CNRS, Faculté de Médecine de Rangueil, 31062 Toulouse CEDEX9, France*

Received 8 February 2007; revised 23 October 2007; accepted 30 October 2007
Available online 7 November 2007

Tonic and phasic dynamics of electroencephalographic (EEG) activities during a continuous compensatory tracking task (CTT) were analyzed using time–frequency analysis of EEG sources identified by independent component analysis (ICA). In 1-hour sessions, 70-channel EEG data were recorded while participants attempted to use frequent compensatory trackball movements to maintain a drifting disc close to a bulls-eye at screen center. Disc trajectories were converted into two moving-average performance measures, root mean square distance of the disc from screen center in 4-s ('local') and in 20-s ('global') moving time windows. Maximally independent EEG processes and their equivalent dipole source locations were obtained using the EEGLAB toolbox (http://sccn.ucsd.edu/eeglab). Across subjects and sessions, independent EEG processes in occipital, somatomotor, and supplementary motor cortices exhibited tonic power increases during periods of high tracking error, plus additional phasic power increases in several frequency bands before and after trackball movements following disc 'perigees' (moments at which the disc began to drift away from the bulls-eye). These phasic activity increases, which were larger during high-error periods, reveal an intimate relation between EEG dynamics and top–down recognition of responding to threatening events. Thus during a continuous tracking task without impulsive stimulus onsets, sub-second scale EEG dynamics related to visuomotor task could be dissociated from slower spectral modulations linked to changes in performance and arousal. We tentatively interpret the observed EEG signal increases as indexing tonic and phasic modulations of the levels of task attention and engagement required to maintain visuomotor performance during sustained performance.

Keywords: EEG; Independent component analysis; Event-related brain dynamics; Visuomotor tracking; Tonic and phasic activities

Introduction

Electroencephalographic (EEG) correlates of fluctuations in human performance and alertness on the order of 1 s to several minutes have been demonstrated (Huang et al., 2001; Jung et al., 1997; Lal and Craig, 2002, 2005; Makeig and Inlow, 1993; Makeig and Jung, 1995, 1996; Makeig et al., 2000; Peiris et al., 2006; Schier, 2000; Tassi et al., 2006). For example, Makeig and Jung (1996) reported that, during drowsiness, success in responding to weak above-threshold auditory targets tended to vary irregularly with cycle lengths of 4 min and longer. These performance fluctuations were accompanied by distinct changes in the power spectrum of the electroencephalogram (EEG) on at least two time scales: (1) mean power at the human sleep spindle frequency (bursts of 12–14 Hz sinusoidal waves that last for 0.5–1.5 s) was tonically elevated during sustained periods of poor or absent performance. (2) During periods of intermittent performance, on average beginning about 10 s before undetected targets, low-theta (4–5 Hz) activity began to increase while gamma band activity (35–40 Hz) decreased. The time courses of these phasic spectral perturbations were paralleled by performance changes in target detection rate. Both spectral power changes and performance returned to baseline about 10 s after the performance lapse, producing circa 20-s cycles of relatively alert and drowsy performance accompanied by compensatory shifts in low-theta and gamma EEG power. During extended periods of drowsiness (as evidenced by poor detection performance), these phasic fluctuations were superimposed on slower tonic changes in both performance and EEG spectrum (Makeig et al., 2000; Makeig and Jung, 1996). However, the auditory stimuli used in the study were discrete and target presentation rate was relatively low (10 per minute). Furthermore, the EEG data were collected at only two scalp sites, not allowing localization of the cortical sources of the observed spectral activity.

Sensory event-related potentials (ERP) index a relatively small proportion of mean electroencephalographic (EEG) activity that

* Corresponding author. Swartz Center for Computational Neuroscience, Institute for Neural Computation, University of California, San Diego, 9500 Gilman Dr. #0961, La Jolla, CA 92093-0961, USA. Fax: +1 858 458 1847.
E-mail address: rshuang@sccn.ucsd.edu (R.-S. Huang).
Available online on ScienceDirect (www.sciencedirect.com).

1053-8119/$ - see front matter © 2007 Elsevier Inc. All rights reserved.
doi:10.1016/j.neuroimage.2007.10.036

becomes phase-locked to onsets of visual or auditory stimuli (Makeig, 1993; Picton et al., 1994). In many ERP paradigms, participants respond to stimulus events with single, discrete button presses. ERP averages are then obtained by averaging time-domain EEG epochs precisely time-locked to stimulus or response onsets. In real life, however, many tasks involve more or less continuous efforts to maintain appropriate performance, instead of occasional impulsive and discretely cued behavioral choices (e.g., selective button presses). During the course of truly continuous performance paradigms, on the other hand, participants may receive continuous visual and/or auditory stimulus streams along with continuous performance feedback (Classen et al., 1998; Contreras-Vidal and Kerick, 2004; Freeman et al., 1999, 2000; Hill and Raab, 2005; Indra et al., 1993; Lal and Craig, 2002, 2005; Mann et al., 1996; Schier, 2000; Sterman and Mann, 1995; Sterman et al., 1994; Ulrich and Kriebitzsch, 1990). In such continuous tasks, onsets of relevant task events (for example, lane drifts during driving simulations) may not be as precisely defined as onsets of visual or auditory stimuli in standard ERP paradigms. Without precisely timed events, it is difficult to identify average ERP features. Furthermore, ERP waveforms, like other EEG measures, may change as the subject's cognitive state changes, e.g., during the process of falling asleep (de Lugt et al., 1996; Ogilvie, 2001). Finally, average ERPs capture only the relatively small percentage of EEG activity that is both time-locked and phase-locked to experimental events. In particular, time-locked changes in spectral power without phase consistency may not appear in ERP measures (Makeig, 1993; Makeig et al., 2002). All these limitations make ERP measures inappropriate or insufficient for assessing event-related brain dynamics in continuous performance tasks accompanied by fluctuating states of arousal and performance.

Another approach to EEG analysis is to investigate event-related oscillatory brain activity with Fourier methods and time–frequency analysis. For instance, Pfurtscheller and colleagues (Neuper and Pfurtscheller, 2001; Pfurtscheller, 1992; Pfurtscheller and Aranibar, 1977; Pfurtscheller and Lopes da Silva, 1999; Pfurtscheller and Neuper, 1994, Pfurtscheller et al., 1996a,b, 1998, 2003, 2005, 2006) showed that rhythmic brain activities in the alpha and beta bands may increase or decrease time-locked to stimulus presentations or movements. Amplitude decreases and increases of ongoing EEG rhythms in particular frequency bands are often referred to as event-related desynchronization (ERD) and synchronization (ERS), respectively. Event-related changes in oscillatory brain activity have been demonstrated in other EEG/MEG studies, including attentional modulation (Babiloni et al., 2004; Fink et al., 2005; Klimesch et al., 1998; Verstraeten and Cluydts, 2002; Worden et al., 2000; Yamagishi et al., 2003, 2005), movements (Jurkiewicz et al., 2006; Parkes et al., 2006; Salmelin and Hari, 1994; Salmelin et al., 1995), cold-induced pain (Backonja et al., 1991), cognitive and memory performance (Bastiaansen et al., 2002; Klimesch, 1999; Onton et al., 2005), and visuomotor tracking tasks (Contreras-Vidal and Kerick, 2004; Indra et al., 1993; Ulrich and Kriebitzsch, 1990).

Most studies of task-related changes in the EEG spectrum have measured spectral power of the EEG signals recorded at individual scalp channels or averaged over collections of nearby scalp channels. Unfortunately, straightforward biophysical modeling shows that most EEG sources, cortical areas with partially synchronized local field potentials, project to nearly all of the scalp electrodes, meaning that EEG electrode recordings contain weighted sums of activities originating in diverse cortical regions. However, creating spatial filters that focus only on one predefined source area and rejecting activities arising from all other source areas may be technically difficult. An alternative method for finding spatial filters for individual sources is provided by independent component analysis (ICA), which builds spatial filters for the maximally distinct (e.g., maximally temporally independent) signals contained in a multichannel EEG recording.

In this study, we applied ICA and event-related spectral perturbation (ERSP) methods (Makeig, 1993), a full-spectrum extension of ERD and ERS measures, to study event-related brain dynamics in a continuous compensatory tracking task (CTT) during which participants attempted to use a trackball to keep a randomly drifting disc in a bulls-eye (target ring) at screen center (Makeig and Jolley, 1996). ICA decomposition was applied to 70-channel EEG data collected in each of three 1-hour CTT sessions per subject (Bell and Sejnowski, 1995; Jung et al., 2001a; Makeig et al., 1996). Maximally independent EEG processes and their dipole source locations were obtained using the EEGLAB toolbox (Delorme and Makeig, 2004; http://sccn.ucsd.edu/eeglab). Mean ERSP responses to disc escapes from screen center were then computed from the time courses of the maximally independent EEG components. The results demonstrate that brain dynamics linked to changes in human performance on the sub-second to many-second time scale can be assessed even in a continuous and interactive tracking task. We report here on three clusters of independent component processes that exhibited significant 'phasic' spectral perturbations following disc trajectory perigees, moments when the moving disc began to drift away from the target ring under the influence of continuously varying forces ('unseen winds'), as well as 'tonic' differences, in several frequency bands, between periods of high and low tracking error. Scalp topographies and mean activity spectra of independent component processes exhibiting these effects were stable across sessions in a small group of subjects.

Materials and methods

Subjects and task

Six right-handed healthy adults (3 males, 3 females; mean age = 27.8, SD = 6.0) with normal or corrected-to-normal vision were paid to participate in the experiment. All subjects gave informed consent before participating in a protocol approved by the Human Research Protections Program of the University of California, San Diego. All subjects had lunch about 2 h before arriving at the laboratory around 2:00 PM. Each subject practiced the task for 20 min to reach satisfactory performance during the placement of the EEG cap and electrodes. Recordings began near 3:00 PM. Subjects sat on a comfortable office chair with armrests and viewed a 19-inch screen placed 50 cm from their eyes in an EEG laboratory room equipped with a light dimmer. The light was set to a fixed luminance level (indicated by a marker on the light switch) at which ordinary text was barely legible. Each subject took part in three 1-hour sessions of a continuous visuomotor compensatory tracking task (CTT) on three different days. No subject reported sleep deprivation the night before the experiment.

The task required subjects to attempt to use a trackball (Fellowes Inc., Itasca, IL) to keep a drifting ('wind-blown') disc as near as possible to a bulls-eye (target ring) at the center of the screen (Fig. 1A) by making frequent (~3/s) movements of the

trackball in the direction of intended movement, producing ('rocket-thrust' like) bursts of directional disc acceleration (Makeig and Jolley, 1996). The perturbation force applied to the disc summed six sine waves with different frequencies (0.05, 0.08, 0.13, 0.21, 0.33, and 0.53 Hz), amplitudes, and random phase angles. Fig. 1B demonstrates sample time courses of the perturbation force, showing multiple local minima during a 15-s period (CTT software and detailed documentation are available at: http://sccn.ucsd.edu/~scott/CTT/CTT.zip and http://www.sccn.ucsd.edu/~scott/pdf/COMPTRACK.pdf).

Subjects were instructed to continue to perform the task as best as they could even if they began to feel drowsy. No intervention was made when subjects occasionally fell asleep and stopped responding. After such non-responsive periods subjects resumed task performance without experimenter intervention. Three of the 18 sessions were rejected for further analysis because of severe noise due to poor skin contacts at the reference electrode or long periods (>40 min) of low performance. The coordinates and dynamics of the drifting disc, and the trackball velocity vector were recorded about 14 times per second via a synchronous pulse marker train that was recorded in parallel by the EEG acquisition system for subsequent analysis.

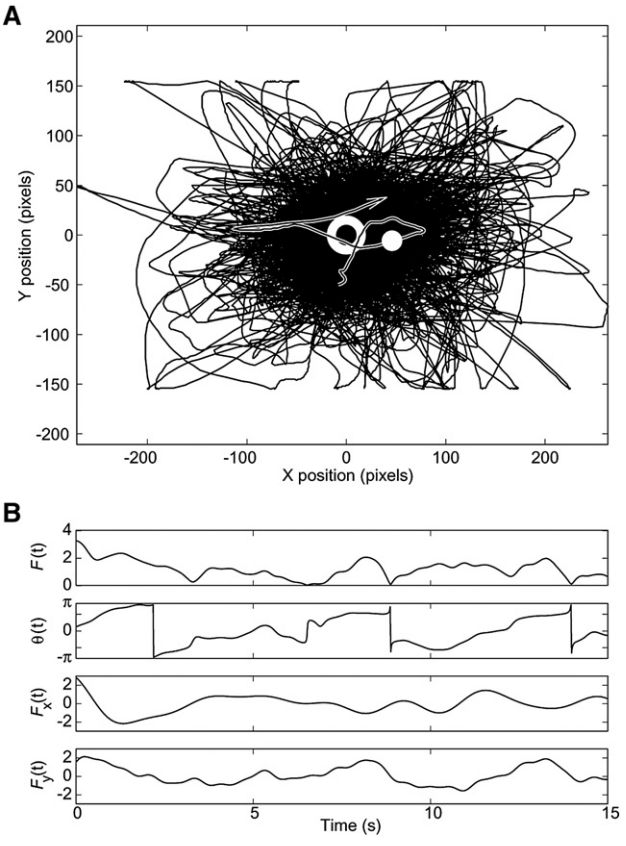

Fig. 1. The compensatory tracking task. (A) Accumulated disc trajectory during a representative one-hour session (SY-1). The white ring represents the bulls-eye target at screen center. The continuous movements of the solid white drifting disc are partially controlled by the subject through thrusting movements of the trackball. The white double lines highlight an 8-s segment of the disc trajectory record. (B) Sample time courses of the perturbation force F, including the amplitude $F(t)$, phase $\theta(t)$, and its 2-D components $F_x(t)$ and $F_y(t)$. Each local minimum in the time course $F(t)$ indicates a moment when the perturbation force begins to increase, resulting in a disc escape (perigee).

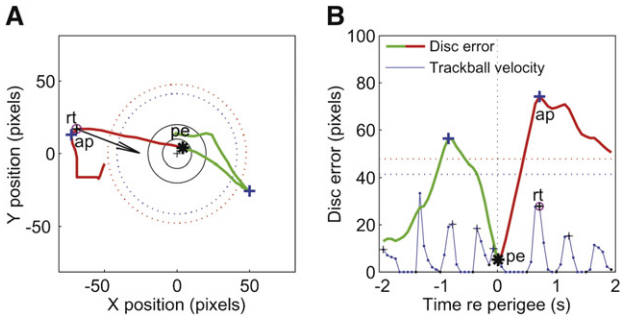

Fig. 2. Analysis of disc trajectory. (A) Disc trajectory in a single 4-s epoch centered on a disc escape. Two concentric black circles represent the bulls-eye pattern (target ring) at screen center. The green and red curves show the 2-s disc trajectory preceding and following a local distance minimum (perigee), marked by a black asterisk (pe). The radii of the red and blue dashed circles respectively show the RMS disc error levels in 4-s and 20-s epochs centered on the perigee. The black arrow represents the direction and magnitude of trackball velocity produced by the subject at a moment (rt) following the illustrated perigee and near the apogee (ap). (B) (Red and green curves) time courses of disc error and (thin blue curves) trackball velocity during the 4-s epoch. Each black cross identifies a subject trackball movement. The black cross in a red circle identifies the first trackball movement ('rt', response time) following the perigee (pe). Other features as in panel A.

Data acquisition

EEG activities were recorded from 70 scalp electrodes. Eye movements and blinks were recorded via two EOG electrodes placed below the right eye and at the left outer canthus, respectively. All electrodes used the right mastoid as reference. EEG and EOG activities were sampled at 250 Hz with an analog pass band of 0.01–100 Hz (SA Instrumentation, San Diego, CA). Data were digitally filtered with a linear 1–45 Hz FIR pass band filter before further analysis.

Analysis of tracking performance

We first illustrate methods for behavioral and EEG data analysis using a representative task session. Fig. 1A demonstrates the accumulated 2-D disc trajectory through the first 1-hour session of subject SY. The recorded time series of disc screen coordinates, $x(t)$ and $y(t)$, were converted into a disc error time series, $d(t)$, defined as the radial distance between the disc and the screen center. Tracking performance was obtained by computing the root mean square (RMS) of $d(t)$ in a moving time window. RMS disc error in a short (4-s) moving window indexed the subject's current ('local') CTT performance, whereas RMS disc error in a long (20-s) window was computed to index longer term ('global') changes in CTT performance.

Fig. 2A shows a segment of the 2-D disc trajectory during a single 4-s period (green and red curves). Fig. 2B shows the disc error time series, $d(t)$, in the same period. A perigee (pe) moment (indicated by an asterisk in Figs. 2A and B) was defined as a local minimum in the disc error time series, $d(t)$. Following perigee moments, the disc began to drift away from the target ring, and subjects attempted to quickly use the trackball to bring the disc

back toward screen center. Note that, in the CTT task, perigee moments do not always occur when the disc is near or on the target ring. Here, each perigee moment was defined as an event onset, and EEG data epochs time-locked to perigee events were extracted. The green and red curves represent the disc trajectory in a 4-s epoch, from 2 s before to 2 s after a disk perigee.

Subjects' motor responses following perigee events were indexed by the 2-D time series of recorded trackball velocity $V(t)$. The blue curve in Fig. 2B represents the magnitude of trackball velocity, each peak representing a trackball movement. The first peak in the trackball velocity time series following a perigee was defined as the subject's response onset (denoted as 'rt' in Fig. 2). In total, 1814 perigees were extracted from this representative session and RMS disc errors were computed for each 4-s (local) and 20-s (global) epoch centered at each perigee. Note that the first valid perigee was selected at least 10 s after the beginning of each session, and the last perigee was selected at least 10 s before the session ended. Fig. 3A shows the time courses of local and global RMS disc error in chronological (time-on-task) order. This 1-hour session included several marked fluctuations in global tracking performance. Fig. 3B demonstrates the same perigee-locked epochs sorted by RMS disc error. Here, near-zero values reflect optimal tracking performance.

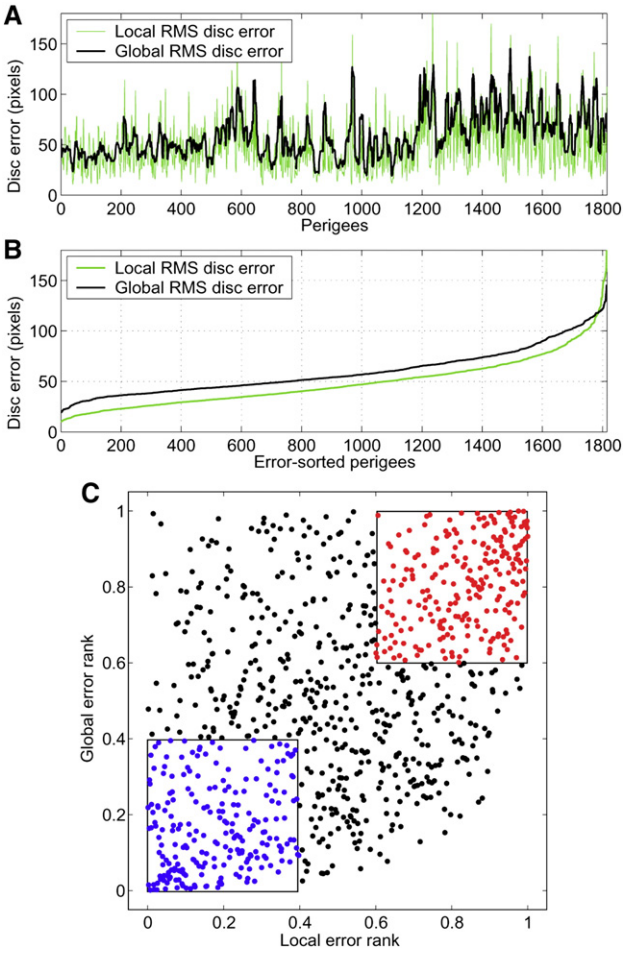

Fig. 3. Analysis of tracking performance. (A) Local (4-s, green curve) and global (20-s, black curve) RMS disc error in 1814 successive perigee-locked epochs from a one-hour session. (B) Sorted global RMS disc error values. (C) Scatter plots of 937 perigees. Each dot indicates the normalized local and global error rank [0, 1] for one perigee. Blue dots: low-error epochs, defined as having both local and global error measures in the lower 40% of epochs. Red dots: high-error epochs, defined as having both local and global error measures in the upper 40%. Black dots: unselected perigees.

Artifact rejection

The numbers of channels included in data analysis for each session and subject are summarized in Table 1. Between 0 and 5 noisy single recording channels per session were removed from the data before analysis because of frequent artifacts arising from poor skin contacts. The compensatory tracking task required continuous effort and frequent (about 3/s) hand and finger movements, sometimes accompanied by head or neck muscle twitch artifacts in the EEG data. During nearly all sessions, subjects yawned a few times. Yawns caused severe artifacts across all channels, which were identified and rejected from the EEG data using available EEGLAB routines (see detailed description at http://www.sccn.ucsd.edu/eeglab/rejtut/tutorialreject.html). Criteria used for artifact rejection included extreme values (fixed thresholds), abnormal trends (linear drifts), and abnormally distributed data (high kurtosis). Epochs contaminated with other sources of artifacts (blinks, eye movements, muscle tension artifacts, and infrequent single-channel noise) were not rejected as these spatially stationary artifacts could be separated from other EEG processes using ICA as described below (Jung et al., 2000, 2001b; Makeig et al., 1996).

Independent component analysis and clustering

Maximally independent EEG processes were obtained using the extended-infomax option of *runica* algorithm from the EEGLAB toolbox (Bell and Sejnowski, 1995; Lee et al., 1999; Makeig et al., 1997). ICA finds an 'unmixing' matrix $\mathbf{W}$ that 'decomposes' or linearly unmixes the multichannel EEG data $\mathbf{x}$ into a sum of maximally temporally independent and spatially fixed components $\mathbf{u}$, where $\mathbf{u}=\mathbf{W}\mathbf{x}$. The rows of the output data matrix $\mathbf{u}$ are time courses of activation of the independent components (ICs). The ICA unmixing matrix $\mathbf{W}$ was trained separately for each session of each subject. Each ICA training set consisted of 2000–3500 s of EEG data from 65 to 70 channels. Initial learning rate was 10^{-4}; training was stopped when the learning rate (a unitless scaling factor) fell below 10^{-6}. From the representative session, SY-1, illustrated above (3322 s, 70 channels), 70 ICs were identified. Some ICs were identified as accounting for blinks, other eye movements, or muscle artifacts according to their scalp maps and activity profiles. Here, we assumed that the dipole source locations of independent components were fixed regardless of tracking performance during each hour-long session.

DIPFIT2 routines from EEGLAB were used to fit single dipole source models to the remaining IC scalp topographies using a four-shell spherical head model (Oostenveld and Oostendorp, 2002). We used the default radii values for the four spheres (71, 72, 79, and 85 mm) and the default conductance values (0.33, 1.0, 0.0042, and 0.33 S/m). In the DIPFIT2 software, the spherical head model is co-registered with an average brain model (Montreal Neurological Institute) and returns approximate Talairach coordinates for each equivalent dipole source (Table 1).

Next, we performed clustering of equivalent ICs across sessions for within-subject analyses and across subjects for between-subject groupings of equivalent ICs (Fig. 4). ICs of interest were selected

and grouped semi-automatically based on their scalp maps, dipole source locations, power spectral baselines, and within-subject consistency (Contreras-Vidal and Kerick, 2004; Jung et al., 2001b; Makeig et al., 2002, 2004a,b; Onton et al., 2005, 2006). To match scalp maps of ICs within and across subjects, the gradients [G_x, G_y] of the IC scalp maps were computed at each electrode location. IC scalp maps from different sessions of the same subject were grouped together based on the highest correlations of gradients for the common electrodes retained in all sessions. Scalp map gradients were then averaged across sessions for each subject and the between-subject correlations were evaluated based on 63 commonly available electrode locations in all subjects and sessions. The correlations between power spectral baselines (102 frequency bins between 0.5 and 49.8 Hz) of IC activities across sessions were also evaluated for each subject. The power spectral baselines of the same IC cluster were then averaged for each subject and between-subject correlations were evaluated.

Epoch selection and epoch segmentation

In each session, each IC activity time series or 'activation' was then separated into 4.5-s time intervals, 1.5 s preceding, and 3 s following each perigee. The average 'inter-perigee-interval' (IPI) in 1814 epochs of the representative session (SY-1) was near 2 s. Three further criteria were employed in final epoch selection. First, perigee-locked epochs contaminated by severe artifacts (excluding blinks and eye movements) were rejected. Second, involuntary finger movements or trackball noise resulted in many brief dips in $d(t)$ that were not significant perigee events. Thus, perigees that were followed by an IPI of less than 1.5 s were rejected from further analysis. Third, epochs in which the subject did not move the trackball between 200 and 2000 ms after the perigee were rejected. Note that trackball responses made between 0 and 200 ms could result from the subject's continuing finger movements or jitters of the trackball itself. Epochs with more than 2000 ms response time were likely due to lapses of responsiveness or microsleeps, during which subjects were not actively engaged in the task. The average number of epochs in all sessions of six subjects was near 1800, of which on average 800 were selected for time–frequency analysis. In session SY-1, for example, 937 out of 1814 perigees met all three criteria and 4.5-s epochs time-locked to these perigees were extracted.

Each of the selected perigee-locked epochs was then associated with two estimates of current performance level, 'local' and 'global' RMS disc errors. An index of tracking performance was then constructed heuristically from these two error estimates. We reasoned that local RMS disc errors alone might not reflect changes of true tracking performance. For instance, a transient response lapse resulting from momentary distraction or an unusual shift in disc acceleration may result in a large local RMS disc error, which could be misinterpreted as microsleeps or lapses of attention. On the other hand, global disc error alone might fail to pick up a quick return to prompt responsiveness. Thus, perigees at which both local and global error ranks were in the lower 40% of the retained epochs were defined as relatively low-error (good performance) periods (Fig. 3C, blue dots), while perigees at which both local and global error ranks were in the upper 40% of the retained epochs were classified as representing high-error (poor performance) periods (Fig. 3C, red dots). In this manner, for session SY-1, 225 (24%) and 235 (25%) of the total 937 perigees were classified as low- and high-error groups, respectively.

Time–frequency analysis and event-related spectral perturbations

IC activities in each epoch were transformed into a (200 latencies by 102 frequencies) time–frequency data matrix using a moving-window average of fast Fourier transforms (FFTs). FFTs were computed for 1-s moving windows centered at 200 evenly spaced latencies from 0.9875 s before to 2.4875 s after the time-locking disk perigee using a data-window length of 256 points (1.024 s), zero-padded to 512 points. Log power spectra were estimated at 102 evenly spaced frequencies from 0.5 Hz to 49.8 Hz and then were normalized by subtracting the log mean power spectral baseline estimated from the pre-perigee period (−1.5–0 s). For each independent component, two event-related spectral perturbation (ERSP) images were thus obtained by averaging all time–frequency images from low- and high-error epochs, respectively. ERSP images were constructed to show potentially significant spectral perturbations (log power differences) from the pre-perigee power spectral baseline ($p<0.01$). Note that, in the continuous tracking task, subjects were attempting to move the disc toward the target ring during the pre-perigee period (baseline). Therefore, the notion of 'baseline period' is different from 'pre-stimulus period' as usually defined in ERP paradigms. Significance of deviations from power spectral baseline was assessed using a nonparametric permutation-based statistical method (Delorme and Makeig, 2004). The mean power spectral baselines for low- and high-error epochs were plotted as thin black and magenta curves, respectively (Fig. 5, middle panels). In the resulting ERSP plots, non-significant time–frequency points were colored green (Fig. 5, left panels).

Tonic and phasic changes in EEG spectrum

Here, we measured the relationships of changes in EEG power spectrum to task performance on two time scales (Klimesch, 1999; Makeig and Jung, 1996). Tonic activity changes refer to changes in EEG power associated with changes in average performance and cognitive state (e.g., arousal) on a longer time scale (sub-minute to minutes). Phasic activity changes refer to event-related brain activity associated with transient performance measured on a shorter time scale (sub-second to seconds). Permutation-based statistics were used to test the significance of tonic differences in power spectral baselines between low- and high-error epochs at each frequency bin. Black horizontal bars (Fig. 5, middle panels) represent frequency ranges exhibiting significant ($p<0.01$) tonic difference between two power spectral baselines. Colored (non-green) areas in the ERSP images (Fig. 5, left panels) signify significant ($p<0.01$) phasic differences between the post-perigee power spectra and the pre-perigee baseline. For both low- and high-error epochs, phasic power spectral maxima (thick blue and red curves in Fig. 5, middle panels) were found for each frequency bin by selecting the maximal value in the ERSP image 0–2.5 s following the perigee. Filled areas and gaps between the power spectral curves represent significant and non-significant maximum values, respectively.

Results

Behavioral performance

All subjects exhibited several high-error periods, sometimes even abandoning control of the trackball altogether in the hour-

Table 1
Dipole source models of independent components

Subjects/Sessions	Number of electrodes	Residual variance (%)	Talairach coordinates			Distance to cluster center (mm)
			x	*y*	*z*	
Occipital cluster						
SY-1	70	2.16	±35	−77	0	2.69
SY-2	69	0.75	±36	−74	−1	1.25
SY-3	70	0.59	±34	−73	−3	2.56
		Mean:	±35	−74.7	−1.3	2.17±0.8
TP-1	70	0.95	±25	−75	9	5.86
TP-2	70	1.53	±27	−73	4	0.82
TP-3	70	1.36	±31	−70	0	6.08
		Mean:	±27.7	−72.7	4.3	4.25±2.98
SS-1	70	3.75	24	−38	−17	*
SS-2	70	3.06	32	−60	9	7.76
SS-3	69	2.25	32	−70	−5	7.76
		Mean:	32	−65	2	8.6
SL-1	65	3.00	40	−71	13	–
		4.44	−38	−54	−2	–
SL-2	67	1.92	±25	−68	4	–
		3.11	33	−78	−3	–
		6.67	−42	−32	−1	–
SL-3	68	4.15	37	−50	−3	–
		2.17	−28	−38	4	–
DG-1	68	3.95	33	−66	27	–
DG-2	68	2.47	−34	−50	−24	–
KH-1	70	3.68	−24	−72	22	–
		2.61	41	−63	16	–
Somatomotor cluster						
SY-1	70	0.97	−33	−27	46	1.25
SY-2	69	1.26	−32	−24	47	2.69
SY-3	70	1.04	−31	−29	47	2.56
		Mean:	−32	−26.7	46.7	2.17±0.8
TP-1	70	1.68	−33	−27	46	10.76
TP-2	70	2.85	−38	−17	48	5.1
TP-3	70	4.36	−30	−8	58	12.42
		Mean:	−33.7	−17.3	50.7	9.43±3.84
SS-1	70	0.93	−27	−32	50	4.29
SS-2	70	1.7	−31	−22	50	7.1
SS-3	69	3.09	−32	−33	48	4.67
		Mean:	−30	−29	49.3	5.35±1.53
SL-1	65	0.93	−20	−20	33	10.4
SL-2	67	3.33	−15	−18	53	13.94
SL-3	68	6.55	−35	−10	40	13.27
		Mean:	−23.3	−16	42	12.54±1.88
DG-1	68	3.08	−21	−21	35	13.87
DG-2	68	0.61	−23	−42	17	13.87
		Mean:	−22	−31.5	26	13.87
KH-1	70	2.61	−53	−34	3	*
		Grand mean:	−28.6	−23.6	44.1	12.57±7.7
Central medial cluster						
SY-1	70	2.86	1	−23	56	4.76
SY-2	69	2.18	−2	−23	56	5.26
SY-3	70	4.55	2	−33	46	9.57
		Mean:	0.33	−26.3	52.7	6.53±2.65
TP-1	70	1.07	−4	−14	52	4.4
TP-2	70	1.18	−4	−33	53	14.76
TP-3	70	0.9	−3	−8	49	10.61
		Mean:	−3.7	−18.3	51.3	9.93±5.22
SS-1	70	2.93	7	−5	34	6.08
SS-2	70	2.9	1	−2	39	6.4
SS-3	69	2.82	−5	−11	29	9.27
		Mean:	1	−6	34	7.25±1.76

(continued on next page)

Table 1 (*continued*)

Subjects/Sessions	Number of electrodes	Residual variance (%)	Talairach coordinates			Distance to cluster center (mm)
			x	*y*	*z*	
Central medial cluster						
SL-1	65	1.87	−4	−7	61	6.22
SL-2	67	12.61	0	32	62	*
SL-3	68	0.96	−1	−2	50	6.22
		Mean:	−2.5	−4.5	55.5	6.22
DG-1	68	1.79	−4	−1	39	5.89
DG-2	68	2.4	−1	−12	42	5.89
		Mean:	−2.5	−6.5	40.5	5.89
KH-1	70	1.46	6	−8	47	–
		Grand mean:	−0.79	−13	46.64	13.22±5.26

*Outlier, not included in within-subject and grand mean results. – Distance to cluster center was not computed because: (1) There was only one session for a subject or (2) some subjects have bilateral dipole models and/or unilateral dipole models on either hemisphere across sessions.

long sessions. Fig. 3A shows that several fluctuations between periods of low and high tracking error occurred in session SY-1.

Independent component (IC) clusters

ICs were selected and clustered based on correlations between their scalp map gradients and on their power spectral baselines across sessions and subjects. Fig. 4 shows the equivalent dipole source locations and scalp maps of 15 sessions (six subjects) for three IC clusters. These three clusters comprised ICs from nearly all sessions and subjects and showed consistent performance-related phasic and tonic changes in IC activations. The residual variances and Talairach coordinates of the equivalent dipole sources of ICs are summarized in Table 1. For each IC cluster, results from the representative session (SY-1) are illustrated in detail (Fig. 5), followed by results from the second session (SY-2) of this subject (Fig. 6A), and from two sessions (TP-1, TP-2) of a second subject (Fig. 6A, B). Fig. 7 shows the grand averages of tonic spectral shifts and prevalence of phasic changes across all 15 sessions for each of the IC clusters, whose spectral characteristics are summarized in Table 2.

Occipital cluster

Fig. 5A shows the scalp map, 2-D/3-D dipole source locations, power spectral baselines and their tonic and phasic shifts, and ERSP images of mean log power changes following disk perigees in low- and high-error epochs for a bilateral occipital IC from session SY-1. The mean ERSP for low-error epochs (Fig. 5A, left panel, lower image) shows that mean power in the high alpha band (near 12 Hz) increased after median onset time (indicated by a red dashed line) of trackball response following disk perigees (phasic changes). Note that the frequency of phasic power increase is above the mean baseline peak frequency (10 Hz), producing a slight upward frequency shift in the alpha peak (Fig. 5A, middle panel). Phasic changes in power at 18–22 Hz in the beta band were smaller than in the alpha band. In high-error epochs, broadband (theta, alpha, and beta bands) phasic changes occurred following disk perigees (Fig. 5A, left panel, upper image). The mean tonic power spectral baseline was significantly larger ($p<0.01$) below 23 Hz in high-error epochs than in low-error epochs (as indicated by black horizontal segments in Fig. 5A, middle panel). Equivalent dipoles in the symmetric source model for this IC were located in the lateral occipital cortex (Fig. 5A, right panel).

Similar patterns of tonic and phasic activity changes were demonstrated for an IC with a nearly identical equivalent dipole model from a second session (SY-2) of the same subject (Fig. 6A, left panel) and from two sessions (TP-1, TP-2) of a second subject, as shown in Figs. 6B and C (left panels), though the power spectral baseline of the second subject did not contain a second peak near 20 Hz.

Fig. 7A shows the grand average of power spectral baselines across six subjects for low- and high-error epochs and the difference (tonic changes) between these two grand mean curves. The power spectral baselines were averaged across sessions within each subject. The reliability of the spectral difference was tested for each frequency bin using nonparametric permutation-based, paired (high- vs. low-error epochs of the same subject) two-tailed *t*-test. Despite variations in EEG recordings across sessions and subjects, grand mean power spectral baseline exhibited significant tonic power increases ($p<0.05$, $n=6$; indicated by green trace segments in Fig. 7A) below 17 Hz and between 19 and 26 Hz in high-error epochs.

Fig. 7B shows, for clustered ICs from the 15 sessions, the grand mean prevalence of the 0–2.5 s period following disk perigee exhibiting significant ($p<0.01$, within each session) phasic changes for each frequency bin. Power spectra in the occipital cluster (Fig. 7B, left panel) showed wideband phasic changes after perigees, with peaks near 10–12 and 20 Hz in both low- and high-error epochs. Phasic changes in low-error epochs were less frequent (occupying on average about 21% of the post-perigee periods) than in high-error epochs (on average ~36%). This prevalence measure can be interpreted as the probability of a significant increase in phasic post-perigee power, across sessions and subjects.

Somatomotor cluster

Fig. 5B shows post-perigee ERSPs, scalp map, 2-D/3-D dipole source locations, and tonic and phasic changes in power spectra for an IC from session SY-1 whose equivalent dipole was located in the left somatomotor cortex, contralateral to the hand manipulating the trackball. The mean perigee-locked ERSP for low-error epochs (Fig. 5B, left panel, lower image) showed a brief increase in (15–25 Hz) beta band power near the perigee followed by a transient increase in low alpha band (8–10 Hz) activity near the median onset time of trackball movements. The ERSP image for high-error epochs (Fig. 5B, left panel, upper image) showed complex sustained increases in EEG activity between 5 and 30 Hz after the perigee that were strongest in the high alpha (near 12 Hz)

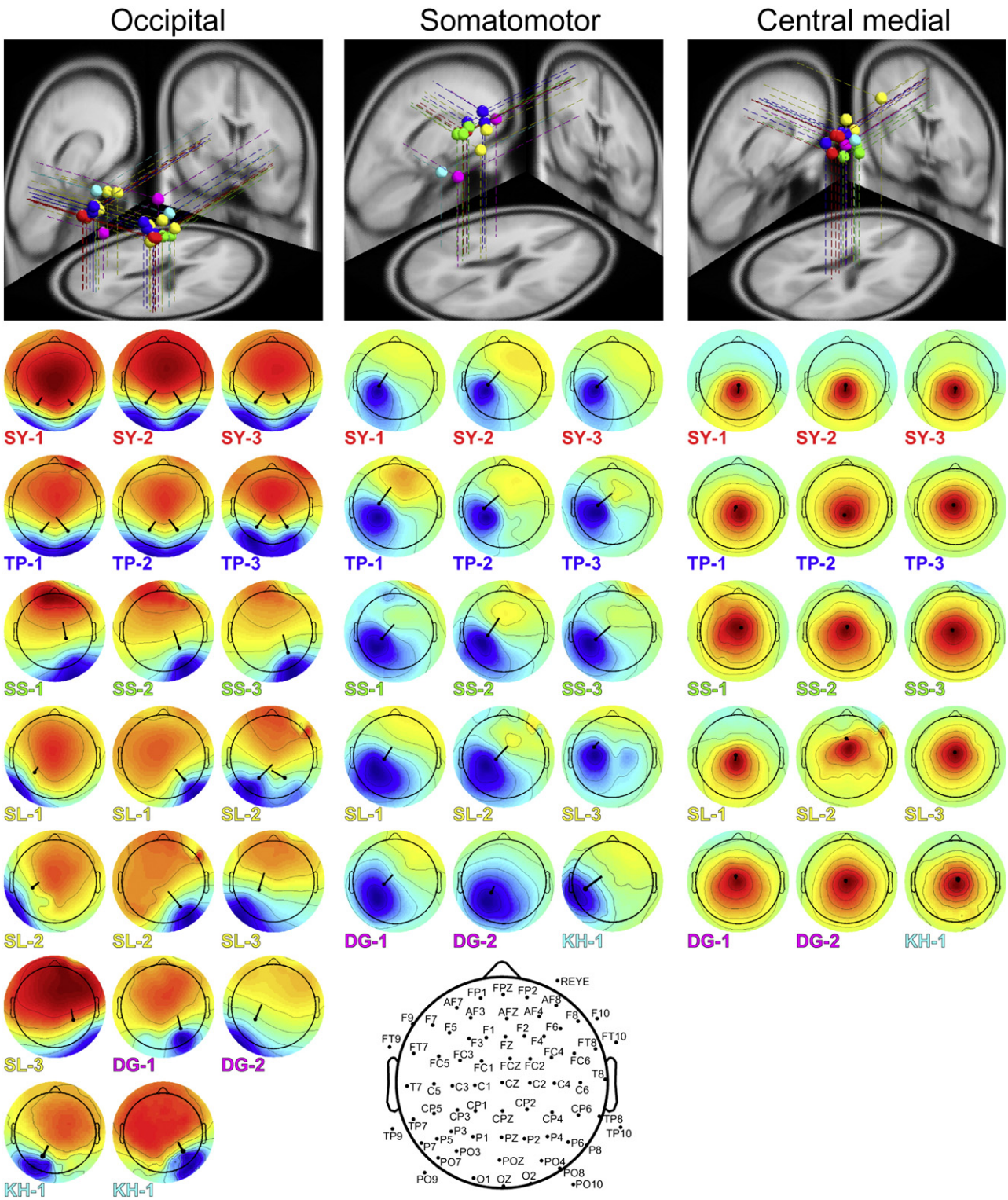

Fig. 4. Equivalent dipole source locations and scalp maps for three independent component (IC) clusters across 15 sessions. (Upper panels) 3-D dipole source locations (colored spheres) and their projections onto average brain images. (Lower panels) Scalp maps and axial-plane dipole locations for cluster ICs from all 15 sessions. Dipole sphere and session labels for each subject have the same color. (Lower middle plot) locations of the 70 EEG and one EOG electrodes in session SY-1.

and beta (near 20 Hz) bands. The mean alpha and beta increases persisted even after the ensuing disc apogee (moment of median local maximum disk distance). Between 7 and 26 Hz, the mean tonic power spectral baseline of high-error epochs was larger than that of low-error epochs, though this difference was significant ($p<0.01$) only in the high alpha band.

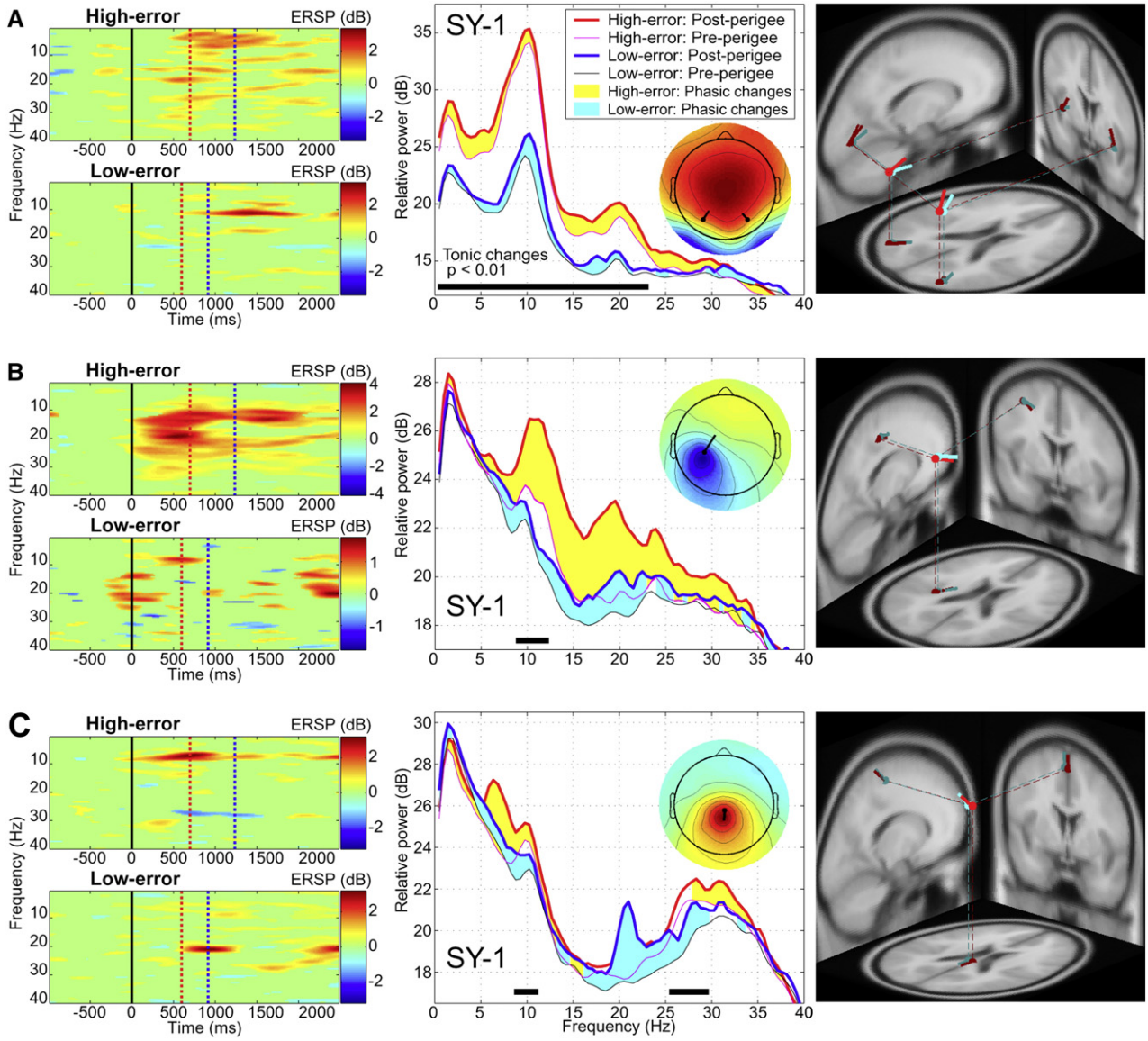

Fig. 5. Single session (SY-1) results. (A) Occipital IC. (B) Somatomotor IC. (C) Central medial IC. (Left panels) Event-related spectral perturbation (ERSP) images of each component. Upper and lower images represent mean ERSPs for high-error and low-error epochs respectively. Black solid lines: disc perigees. Red dashed lines: median time of first trackball response. Blue dashed lines: median time of ensuing local distance maximum (apogee). (Middle panels) IC scalp maps and equivalent dipole locations, plus tonic and phasic power spectra. Thin black and magenta curves: mean spectral power baselines preceding disc perigees in low-error and high-error epochs, respectively. Thick blue and red curves: maximum ERSP power in the 0–2.5 s following perigees. Yellow and cyan fills: frequency ranges exhibiting significant ($p<0.01$) phasic post-perigee power increases in high-error and low-error epochs, respectively. (Black horizontal line segments) Frequencies exhibiting significant ($p<0.01$) tonic spectral power increases (high-error minus low-error). (Right panels) Equivalent dipole IC source locations and their projections onto average brain images. Red and cyan pins: equivalent-dipole locations and moments for best-matching IC pairs from sessions SY-1 and SY-2 (see Fig. 6A).

Similar patterns of tonic and phasic activity were found for an IC in the left somatomotor area from the second session (SY-2) of the same subject (Fig. 6A, middle panel), as well as for two sessions (TP-1, TP-2) of a second subject (Figs. 6B and C, middle panels). Equivalent dipole locations of the somatomotor cluster were similar across sessions (Fig. 4, middle panel; Fig. 5B, right panel). In all four sessions shown, significant tonic increases in EEG power between 7 and 28 Hz occurred in high-error epochs relative to low-error epochs. Post-perigee phasic increases were significant ($p<0.01$) in theta, alpha, and beta bands in high-error epochs.

The grand average of power spectral baselines showed tonic increases below 30 Hz in high-error relative to low-error epochs, and the mean difference was significant ($p<0.05$, $n=6$) between 3–6, 11–17, and 19–30 Hz (Fig. 7A, middle panel). In high-error epochs, significant ($p<0.01$, within each session) phasic increases occupied about 20–43% of the post-perigee period (0–2.5 s) across all frequencies, particularly at alpha and beta bands (Fig. 7B, middle panel). The phasic increases in low-error epochs were wideband and less prevalent (~15% on average).

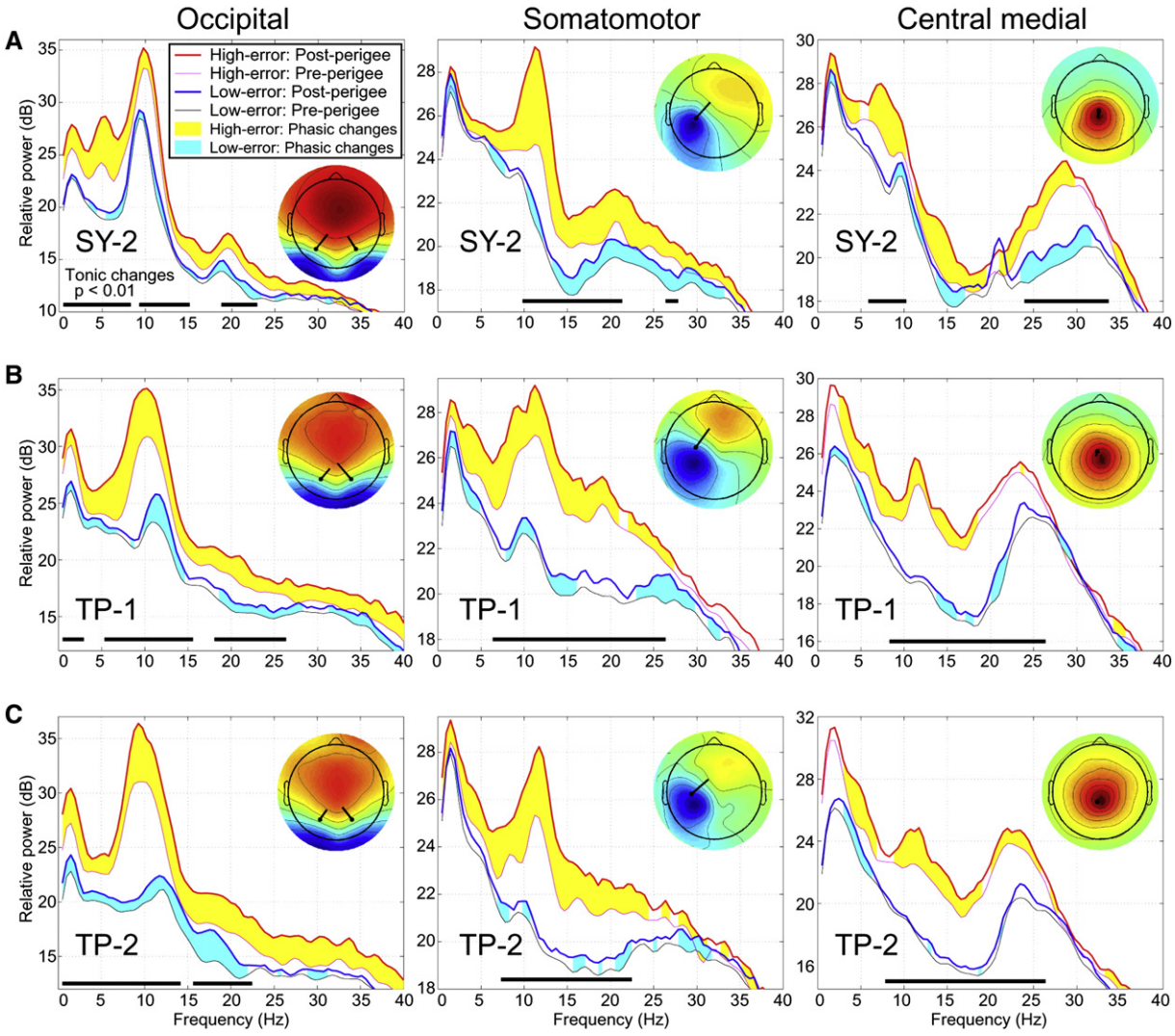

Fig. 6. Within-subject and between-subject IC scalp maps and tonic/phasic power spectral changes in low-error and high-error epochs. (Left panels) occipital cluster ICs; (middle panels) somatomotor cluster ICs; (right panels) central medial cluster ICs for sessions: (A) SY-2, (B). TP-1, and (C) TP-2. Other details as in Fig. 5.

Central medial cluster

Fig. 5C shows the ERSPs, scalp map, 2-D/3-D dipole source locations, and tonic and phasic changes in the power spectrum of an IC process in session SY-1 projecting most strongly to the central midline. The equivalent dipole model for this IC was located in or near the supplementary motor area (SMA) (Fig. 5C, right panel). The mean ERSP for low-error epochs (Fig. 5C, left panel, lower image) showed phasic post-perigee increases in power in the low alpha band (8–10 Hz) in high-error epochs, while in low-error epochs a phasic increase in power near 25 Hz appeared from the moment of median time of response onset to the median time of disc apogee.

In the alpha and high beta bands (8–12 Hz and 25–30 Hz), mean tonic baseline power in high-error epochs was significantly ($p<0.01$) larger than in low-error epochs. Similar patterns of tonic and phasic activity differences were observed in a central medial IC from a second session (SY-2) of the same subject (Fig. 6A, right panel). Results from two sessions (TP-1, TP-2) of the second subject showed wideband (theta, alpha, and beta) phasic increases in high-error epochs (Figs. 6B and C, right panels) in addition to significant ($p<0.01$) tonic changes between 7 and 27 Hz in both sessions.

Across subjects, the grand mean of power spectral baselines showed significant ($p<0.05$, $n=6$) tonic increases between 13–17 and 19–32 Hz in high-error relative to low-error epochs (Fig. 7A, right panel), while the grand mean prevalence (on average ~18%) of significant ($p<0.01$, within each session) phasic post-perigee power increases (Fig. 7B, right panel) was larger in 4–7 Hz theta and 8–12 Hz alpha bands during high-error epochs. ERSPs of low-error epochs contained scattered wideband phasic power increases on average ~15% of the post-perigee periods (0–2.5 s), with an apparent peak near 28 Hz.

Discussion

In this study, we analyzed slowly varying (tonic) and quickly varying (phasic) shifts in EEG spectral dynamics during a con-

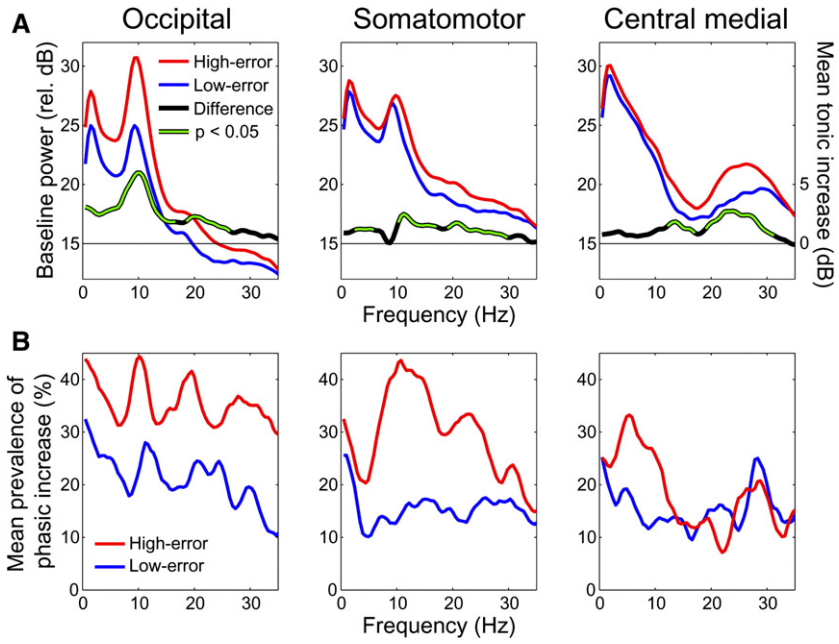

Fig. 7. Grand averages of tonic and phasic spectral changes. (A) Grand mean power spectral baselines for three IC clusters (left, center and right panels) across ICs from six subjects. Left axis: mean power spectral baselines of (blue curves) low-error and (red curves) high-error epochs. Right axis: (green/black curves) high-error minus low-error power spectral difference. Significant ($p<0.05$, $n=6$) tonic differences are indicated in green trace segments. (B) Mean prevalence (in percentage) of the 0–2.5 s post-perigee period with significant ($p<0.01$, within each session) phasic (post-perigee minus pre-perigee) power increases, averaged across all sessions for each IC. Blue curves: low-error epochs. Red curves: high-error epochs.

tinuous visuomotor tracking task using independent component analysis, time–frequency analysis, and nonparametric permutation-based statistics, demonstrating methods for modeling fluctuations in spectral dynamics of maximally independent EEG processes on different time scales during continuous task performance.

In most ERP paradigms, participants wait passively to respond to impulsively presented stimuli with discrete button presses. ERP analysis requires that EEG epochs be precisely phase-locked to stimulus or response events and, in effect, models the baseline period preceding stimulus onsets as electrically 'silent.' In this study, during performance of the continuous compensatory tracking task, participants were required to continuously attend to the location of the drifting disc and actively try to compensate for its random wandering with roughly 3/s graded finger movements without central gaze fixation. The challenging task events (i.e., disc escapes at perigees) prompting the phasic EEG activities increases appeared when the disc was at any screen position. They were not announced by any sudden (e.g., stimulus onset) event and required a rapid series of trackball movements in responding to return the disc to the bulls-eye target at screen center. As the task comprised no abrupt stimulus onsets, assessing time- and phase-locked average sensory stimulus event-related potential (ERP) features was not possible. However, disc perigees (moments at which the disc drifted away from the target ring at screen center) were critical moments at which participants needed to promptly compensate for the drift event using appropriate finger movements. Therefore, to characterize performance-related EEG dynamics, disc perigees were identified *post hoc* from the disc trajectories and perigee time-locked epochs were extracted from the EEG data and subjected to time–frequency analysis after spatial filtering.

Clean separation of EEG data into functionally and anatomically distinct processes has traditionally been difficult or impossible. Because of volume conduction through brain tissue, cerebrospinal fluid, skull, and scalp, activities arising from multiple brain networks all contribute to EEG data collected anywhere on the scalp. In addition, blinks, eye movements, and muscle artifacts may also contaminate EEG data. These factors make it difficult to relate distinct EEG patterns, originating in specific brain areas, to

Table 2
Summary of spectral characteristics of three independent component clusters

	Occipital cluster	Somatomotor cluster	Central medial cluster
Dominant frequency in power spectral baselines (low-error epochs)	Alpha	Alpha (mu)	20–30 Hz
Tonic changes	<23 Hz	Alpha, ~20 Hz	8–26 Hz
(High-error minus low-error epochs)	(15/15 sessions)	(12/15 sessions)	(11/15 sessions)
Phasic changes	Wideband	Alpha, 13–30 Hz	Theta, alpha, ~30 Hz
(High-error epochs)	(14/15 sessions)	(12/15 sessions)	(10/15 sessions)

Note. Each numerator represents number of sessions exhibiting significant tonic changes ($p<0.01$, within each session) or phasic changes ($p<0.01$, within each session) in the frequency bands specified above.

behavior or pathology, or to identify the brain origins of distinct EEG sources. In particular, because of common volume conduction from nearly any cortical area to nearly any scalp electrode, spectral analysis of EEG data measured directly at scalp sensors is typically confounded.

In this study, we used ICA to blindly separate multichannel data sets into statistically maximally independent components (ICs) arising from distinct or overlapping brain and extra-brain networks (e.g., eye, muscle, and heart activities). Time–frequency analysis could then be applied to the activations of EEG source signals as opposed to mixtures of EEG activities, minimizing potential confounds arising from volume conduction and summation of source signals at the scalp sensors. Results of this analysis showed that EEG dynamics in multiple cortical IC source areas were altered following disc perigees. We found statistically reliable phasic increases in the power spectra of IC process activities that occurred following disc perigees, particularly during high-error periods and putatively drowsy performance. These phasic power increases appeared over a wide frequency range, from 1 Hz to at least 30 Hz, depending on the location and spectral characteristics of the IC process, and lasted from a few hundred milliseconds to 1 s or longer. During periods of poor performance that we interpreted as indicating a state of relative drowsiness, these phasic increases were superimposed on longer lasting or tonic spectral increases.

Appearance of alpha activity has long been noted to accompany relaxed wakefulness or incipient transition from wakefulness to drowsiness. Similarly, alpha activities increase and then start to decrease during increasing drowsiness leading to sleep onset (Cantero et al., 1999, 2002; Ogilvie, 2001; Ogilvie and Harsh, 1995; Santamaria and Chiappa, 1987). In the occipital IC cluster we observed three performance-related effects on mean alpha band power. First, during low-error periods, following disc perigees alpha power increased transiently ('phasically') after response onsets. Second, during high-error periods, baseline alpha band power was significantly ('tonically') larger than during low-error periods. Third, a further phasic increase was observed following disc perigees during high-error periods. The tonic baseline increases during high-error periods were typically larger than the post-perigee phasic increases during low-error performance. These modifications of alpha activities occurred during a continuous visuomotor task in which the subject exhibited fluctuations in performance and arousal. Since transient (phasic) alpha activities tended to increase or decrease relative to the changing tonic alpha baseline following task-relevant events in both low-error and high-error periods, absolute alpha band power estimated near event moments does not suffice as an index of arousal during continuous task performance. Also, roughly 20-s cycles in low-theta-band EEG power may appear during periods of frankly drowsy, intermittent performance (Makeig and Jung, 1996; Makeig et al., 2000). Thus, spectral power changes in low theta band estimated using a longer time window of 20 s or more may provide better estimate of operant arousal.

EEG processes in the left somatomotor and central medial IC clusters also exhibited small tonic increases above 10 Hz during high-error periods (Fig. 7A). These included an apparent slight upward shift, during high-error periods epochs, in the frequency of the somatomotor alpha or mu rhythm. The performance-related tonic changes in the somatomotor and supplementary motor area IC clusters were less prominent than tonic changes in the occipital IC cluster, which occurred predominantly below 12 Hz.

In the left somatomotor IC cluster, phasic post-perigee increases in alpha and beta band power were more prominent in high-error epochs than in low-error epochs (Fig. 5B; Fig. 6, middle panel). These phasic activities might be related to event-related synchronization (ERS) observed following intentional movements (Pfurtscheller and Neuper, 1994, Pfurtscheller et al., 1996a,b, 1998, 2003, 2005; Jurkiewicz et al., 2006; Parkes et al., 2006; Salmelin and Hari, 1994; Salmelin et al., 1995). Our results showed, however, that the phasic increases in IC activity began before the first movement onset following the perigee and persisted through the compensatory maneuver.

The tonic increases in power spectrum from low-error to high-error epochs were consistently observed across subjects, while the phasic post-perigee increases varied more across subjects. This may possibly be linked to an uncertainty in identifying the disc perigees to which subjects reacted most actively. Similar tonic and phasic EEG dynamic features have been observed in a compensatory simulated driving task (Huang et al., 2005) in which participants attempted to remain at the center of a cruising lane during computer-simulated lane drifts. The onsets of these lane drifts were less frequent, more precisely marked, and more perceptually salient than many of the disc perigees in the compensatory tracking task. In that study, tonic alpha power also increased during periods of relatively poor driving performance, and transient decrease and increase in alpha band, sometimes referred to in the EEG literature as an alpha suppression and rebound, or event-related desynchronization and synchronization (ERD/ERS), were observed in IC processes originating in the lateral occipital cortex following each compensatory steering event. The data analysis techniques demonstrated here might be useful for studying event-related brain dynamics in other 'real-world' continuous performance tasks.

What is the functional significance, if any, of the increases in oscillatory EEG activity we observed during periods of high-error performance? During drowsiness, as indexed by performance drop-offs, tonic scalp EEG power has been found to be higher on average than during waking, but most reliably so only at low-theta frequencies near 4 Hz (Makeig and Inlow, 1993). Makeig and Jung (1996) also found that, during periods of intermittent performance, large phasic alpha and beta band post-event increases followed targets that elicited no behavioral response. Tonic and/or phasic increases in EEG power during increased attention to the task in low-error performance periods might be expected at beta and gamma frequencies, given their frequent association with focused attention (Engel et al., 2001; Klimesch, 1999; Ward, 2003; Worden et al., 2000). Here, as in our earlier experiments (Makeig and Jung, 1995, 1996), participants may have increased the level of their 'cognitive effort' or 'attention to the task' in response to the increased level of performance challenge posed by normal task demands during drowsiness (Wu et al., 1999), a phenomenon that might also be related to the phasic increase in theta band power during high-error epochs in the central medial IC cluster (Fig. 7B, right panel). Increases in occipital and somatomotor alpha band rhythms, on the other hand, have been associated with voluntary and selective decreases in visual and somatomotor attention (Bauer et al., 2006; Worden et al., 2000), possibly accounting for the consistent increases in tonic alpha power in occipital and somatomotor IC clusters during high-error periods (Fig. 7A, left and middle panels). To conclude, our results suggest that detailed study on changes in the EEG power spectrum during continuous performance must take into account that these EEG changes occur

at many frequencies on multiple time scales and differ between brain areas.

Acknowledgments

This research was supported by a gift from The Swartz Foundation (Old Field, NY) and by grants from National Aeronautics and Space Administration (NASA) and DENSO Corp. (Japan). We thank Terrence J. Sejnowski for discussion and comments and Julie Onton for help with experiments and data analysis.

References

Babiloni, C., Miniussi, C., Babiloni, F., Carducci, F., Cincotti, F., Del Percio, C., Sirello, G., Fracassi, C., Nobre, A.C., Rossini, P.M., 2004. Subsecond "temporal attention" modulates alpha rhythms. A high-resolution EEG study. Brain Res. Cogn. Brain Res. 19, 259–268.

Backonja, M., Howland, E.W., Wang, J., Smith, J., Salinsky, M., Cleeland, C.S., 1991. Tonic changes in alpha power during immersion of the hand in cold water. Electroencephalogr. Clin. Neurophysiol. 79, 192–203.

Bastiaansen, M.C., Posthuma, D., Groot, P.F., de Geus, E.J., 2002. Event-related alpha and theta responses in a visuo-spatial working memory task. Clin. Neurophysiol. 113, 1882–1893.

Bauer, M., Oostenveld, R., Peeters, M., Fries, P., 2006. Tactile spatial attention enhances gamma-band activity in somatosensory cortex and reduces low-frequency activity in parieto-occipital areas. J. Neurosci. 26, 490–501.

Bell, A.J., Sejnowski, T.J., 1995. An information-maximization approach to blind separation and blind deconvolution. Neural. Comput. 7, 1129–1159.

Cantero, J.L., Atienza, M., Salas, R.M., Gomez, C.M., 1999. Brain spatial microstates of human spontaneous alpha activity in relaxed wakefulness, drowsiness period, and REM sleep. Brain Topogr. 11, 257–263.

Cantero, J.L., Atienza, M., Salas, R.M., 2002. Human alpha oscillations in wakefulness, drowsiness period, and REM sleep: different electroencephalographic phenomena within the alpha band. Neurophysiol. Clin. 32, 54–71.

Classen, J., Gerloff, C., Honda, M., Hallett, M., 1998. Integrative visuomotor behavior is associated with interregionally coherent oscillations in the human brain. J. Neurophysiol. 79, 1567–1573.

Contreras-Vidal, J.L., Kerick, S.E., 2004. Independent component analysis of dynamic brain responses during visuomotor adaptation. NeuroImage 21, 936–945.

Delorme, A., Makeig, S., 2004. EEGLAB: an open source toolbox for analysis of single-trial EEG dynamics including independent component analysis. J. Neurosci. Methods 134, 9–21.

de Lugt, D.R., Loewy, D.H., Campbell, K.B., 1996. The effect of sleep onset on event related potentials with rapid rates of stimulus presentation. Electroencephalogr. Clin. Neurophysiol. 98, 484–492.

Engel, A.K., Fries, P., Singer, W., 2001. Dynamic predictions: oscillations and synchrony in top–down processing. Nat. Rev., Neurosci. 2, 704–716.

Fink, A., Grabner, R.H., Neuper, C., Neubauer, A.C., 2005. EEG alpha band dissociation with increasing task demands. Brain Res. Cogn. Brain Res. 24, 252–259.

Freeman, F.G., Mikulka, P.J., Prinzel, L.J., Scerbo, M.W., 1999. Evaluation of an adaptive automation system using three EEG indices with a visual tracking task. Biol. Psychol. 50, 61–76.

Freeman, F.G., Mikulka, P.J., Scerbo, M.W., Prinzel, L.J., Clouatre, K., 2000. Evaluation of a psychophysiologically controlled adaptive automation system, using performance on a tracking task. Appl. Psychophysiol. Biofeedback 25, 103–115.

Hill, H., Raab, M., 2005. Analyzing a complex visuomotor tracking task with brain-electrical event related potentials. Hum. Mov. Sci. 24, 1–30.

Huang, R.S., Tsai, L.L., Kuo, C.J., 2001. Selection of valid and reliable EEG features for predicting auditory and visual alertness levels. Proc. Natl. Sci. Counc. Repub. China B Life Sci. 25, 17–25.

Huang, R.S., Jung, T.P., Duann, J.R., Makeig, S., Sereno, M.I., 2005. Imaging brain dynamics during continuous driving using independent component analysis. Proc. 35th Annual Meeting of the Society for Neuroscience, Washington D.C.

Indra, M., Bohdanecky, Z., Radil, T., 1993. EEG changes related to one-dimensional hand-tracking. Int. J. Psychophysiol. 15, 59–65.

Jung, T.P., Makeig, S., Stensmo, M., Sejnowski, T.J., 1997. Estimating alertness from the EEG power spectrum. IEEE Trans. Biomed. Eng. 44, 60–69.

Jung, T.P., Humphries, C., Lee, T.W., McKeown, M.J., Iragui, V., Makeig, S., Sejnowski, T.J., 2000. Removing electroencephalographic artifacts by blind source separation. Psychophysiology 37, 163–178.

Jung, T.P., Makeig, S., McKeown, M.J., Bell, A.J., Lee, T.W., Sejnowski, T.J., 2001a. Imaging brain dynamics using independent component analysis. Proc. IEEE 89, 1107–1122.

Jung, T.P., Makeig, S., Westerfield, W., Townsend, J., Courchesne, E., Sejnowski, T.J., 2001b. Analysis and visualization of single-trial event-related potentials. Hum. Brain Mapp. 14, 166–185.

Jurkiewicz, M.T., Gaetz, W.C., Bostan, A.C., Cheyne, D., 2006. Post-movement beta rebound is generated in motor cortex: evidence from neuromagnetic recordings. NeuroImage 32, 1281–1289.

Klimesch, W., 1999. EEG alpha and theta oscillations reflect cognitive and memory performance: a review and analysis. Brain Res. Brain Res. Rev. 29, 169–195.

Klimesch, W., Doppelmayr, M., Russegger, H., Pachinger, T., Schwaiger, J., 1998. Induced alpha band power changes in the human EEG and attention. Neurosci. Lett. 244, 73–76.

Lal, S.K., Craig, A., 2002. Driver fatigue: electroencephalography and psychological assessment. Psychophysiology 39, 313–321.

Lal, S.K., Craig, A., 2005. Reproducibility of the spectral components of the electroencephalogram during driver fatigue. Int. J. Psychophysiol. 55, 137–143.

Lee, T.W., Girolami, M., Sejnowski, T.J., 1999. Independent component analysis using an extended infomax algorithm for mixed sub-Gaussian and super-Gaussian sources. Neural. Comput. 11, 609–633.

Makeig, S., 1993. Auditory event-related dynamics of the EEG spectrum and effects of exposure to tones. Electroencephalogr. Clin. Neurophysiol. 86, 283–293.

Makeig, S., Inlow, M., 1993. Lapses in alertness: coherence of fluctuations in performance and the EEG spectrum. Electroencephalogr. Clin. Neurophysiol. 86, 23–35.

Makeig, S., Jolley, M., 1996. COMPTRACK: a compensatory tracking task for monitoring alertness. Technical Document 96-3C Naval Health Research Center, San Diego.

Makeig, S., Jung, T.P., 1995. Changes in alertness are a principal component of variance in the EEG spectrum. NeuroReport 7, 213–216.

Makeig, S., Jung, T.P., 1996. Tonic, phasic and transient EEG correlates of auditory awareness in drowsiness. Cogn. Brain Res. 4, 15–25.

Makeig, S., Bell, A.J., Jung, T.P., Sejnowski, T.J., 1996. Independent component analysis of electroencephalographic data. Adv. Neural Info. Process. Syst. 8, 145–151.

Makeig, S., Jung, T.P., Bell, A.J., Ghahremani, D., Sejnowski, T.J., 1997. Blind separation of auditory event-related brain responses into independent components. Proc. Natl. Acad. Sci. U. S. A. 94, 10979–10984.

Makeig, S., Jung, T.P., Sejnowski, T.J., 2000. Awareness during drowsiness: dynamics and electrophysiological correlates. Can. J. Exp. Psy. 54, 266–273.

Makeig, S., Westerfield, M., Jung, T.P., Enghoff, S., Townsend, J., Courchesne, E., Sejnowski, T.J., 2002. Dynamic brain sources of visual evoked responses. Science 295, 690–694.

Makeig, S., Delorme, A., Westerfield, M., Jung, T.P., Townsend, J., Courchesne, E., Sejnowski, T.J., 2004a. Electroencephalographic brain dynamics following manually responded visual targets. PLoS Biol. 2, 747–762.

Makeig, S., Debener, S., Onton, J., Delorme, A., 2004b. Mining event-related brain dynamics. Trends Cogn. Sci. 8, 204–210.
Mann, C.A., Sterman, M.B., Kaiser, D.A., 1996. Suppression of EEG rhythmic frequencies during somato-motor and visuo-motor behavior. Int. J. Psychophysiol. 23, 1–7.
Neuper, C., Pfurtscheller, G., 2001. Event-related dynamics of cortical rhythms: frequency-specific features and functional correlates. Int. J. Psychophysiol. 43, 41–58.
Ogilvie, R.D., 2001. The process of falling asleep. Sleep Med. Rev. 5, 247–270.
Ogilvie, R.D., Harsh, J.R. (Eds.), 1995. Sleep onset: normal and abnormal processes. American Psychological Association, Washington.
Onton, J., Delorme, A., Makeig, S., 2005. Frontal midline EEG dynamics during working memory. NeuroImage 27, 341–356.
Onton, J., Westerfield, M., Townsend, J., Makeig, S., 2006. Imaging human EEG dynamics using independent component analysis. Neurosci. Biobehav. Rev. 30, 808–822.
Oostenveld, R., Oostendorp, T.F., 2002. Validating the boundary element method for forward and inverse EEG computations in the presence of a hole in the skull. Hum. Brain Mapp. 17, 179–192.
Parkes, L.M., Bastiaansen, M.C., Norris, D.G., 2006. Combining EEG and fMRI to investigate the post-movement beta rebound. NeuroImage 29, 685–696.
Peiris, M.T., Jones, R.D., Davidson, P.R., Carroll, G.J., Bones, P.J., 2006. Frequent lapses of responsiveness during an extended visuomotor tracking task in non-sleep-deprived subjects. J. Sleep Res. 15, 291–300.
Picton, T.W., Lins, O.G., Scherg, M., 1994. The recording and analysis of event-related potentials. In: Boller, F., Grafman, J. (Eds.), Handbook of Neurophysiology, vol. 9. Elsevier Science, Amsterdam, pp. 429–499.
Pfurtscheller, G., 1992. Event-related synchronization (ERS) an electrophysiological correlate of cortical areas at rest. Electroencephalogr. Clin. Neurophysiol. 83, 62–69.
Pfurtscheller, G., Aranibar, A., 1977. Event-related cortical desynchronization detected by power measurements of scalp EEG. Electroencephalogr. Clin. Neurophysiol. 42, 817–826.
Pfurtscheller, G., Lopes da Silva, F.H., 1999. Event-related EEG/MEG synchronization and desynchronization: basic principles. Clin. Neurophysiol. 110, 1842–1857.
Pfurtscheller, G., Neuper, C., 1994. Event-related synchronization of mu rhythm in the EEG over the cortical hand area in man. Neurosci. Lett. 174, 93–96.
Pfurtscheller, G., Stancak Jr., A., Neuper, C., 1996a. Event-related synchronization (ERS) in the alpha band—an electrophysiological correlate of cortical idling: a review. Int. J. Psychophysiol. 24, 39–46.
Pfurtscheller, G., Stancak Jr., A., Neuper, C., 1996b. Post-movement beta synchronization. A correlate of an idling motor area? Electroencephalogr. Clin. Neurophysiol. 98, 281–293.
Pfurtscheller, G., Zalaudek, K., Neuper, C., 1998. Event-related beta synchronization after wrist, finger and thumb movement. Electroencephalogr. Clin. Neurophysiol. 109, 154–160.
Pfurtscheller, G., Woertz, M., Supp, G., Lopes da Silva, F.H., 2003. Early onset of post-movement beta electroencephalogram synchronization in the supplementary motor area during self-paced finger movement in man. Neurosci. Lett. 339, 111–114.
Pfurtscheller, G., Neuper, C., Brunner, C., Lopes da Silva, F.H., 2005. Beta rebound after different types of motor imagery in man. Neurosci. Lett. 378, 156–159.
Pfurtscheller, G., Brunner, C., Schlogl, A., Lopes da Silva, F.H., 2006. Mu rhythm (de)synchronization and EEG single-trial classification of different motor imagery tasks. NeuroImage 31, 153–159.
Salmelin, R., Hari, R., 1994. Spatiotemporal characteristics of sensorimotor neuromagnetic rhythms related to thumb movement. Neuroscience 60, 537–550.
Salmelin, R., Hamalainen, M., Kajola, M., Hari, R., 1995. Functional segregation of movement-related rhythmic activity in the human brain. NeuroImage 2, 237–243.
Santamaria, J., Chiappa, K.H. (Eds.), 1987. The EEG of drowsiness. Demos, New York.
Schier, M.A., 2000. Changes in EEG alpha power during simulated driving: a demonstration. Int. J. Psychophysiol. 37, 155–162.
Sterman, M.B., Mann, C.A., 1995. Concepts and applications of EEG analysis in aviation performance evaluation. Biol. Psychol. 40, 115–130.
Sterman, M.B., Mann, C.A., Kaiser, D.A., Suyenobu, B.Y., 1994. Multiband topographic EEG analysis of a simulated visuomotor aviation task. Int. J. Psychophysiol. 16, 49–56.
Tassi, P., Bonnefond, A., Engasser, O., Hoeft, A., Eschenlauer, R., Muzet, A., 2006. EEG spectral power and cognitive performance during sleep inertia: the effect of normal sleep duration and partial sleep deprivation. Physiol. Behav. 87, 177–184.
Ulrich, G., Kriebitzsch, R., 1990. Visuomotor tracking performance and task-induced modulation of alpha activity. Int. J. Psychophysiol. 10, 199–202.
Verstraeten, E., Cluydts, R., 2002. Attentional switching-related human EEG alpha oscillations. NeuroReport 13, 681–684.
Ward, L.M., 2003. Synchronous neural oscillations and cognitive processes. Trends. Cogn. Sci. 7, 553–559.
Worden, M.S., Foxe, J.J., Wang, N., Simpson, G.V., 2000. Anticipatory biasing of visuospatial attention indexed by retinotopically specific alpha-band electroencephalography increases over occipital cortex. J. Neurosci. 20 (RC63), 1–6.
Wu, J., Buchsbaum, M.S., Gillin, J.C., Tang, C., Cadwell, S., Wiegand, M., Najafi, A., Klein, E., Hazen, K., Bunney Jr., W.E., Fallon, J.H., Keator, D., 1999. Prediction of antidepressant effects of sleep deprivation by metabolic rates in the ventral anterior cingulate and medial prefrontal cortex. Am. J. Psychiatry 156, 1149–1158.
Yamagishi, N., Callan, D.E., Goda, N., Anderson, S.J., Yoshida, Y., Kawato, M., 2003. Attentional modulation of oscillatory activity in human visual cortex. NeuroImage 20, 98–113.
Yamagishi, N., Goda, N., Callan, D.E., Anderson, S.J., Kawato, M., 2005. Attentional shifts towards an expected visual target alter the level of alpha-band oscillatory activity in the human calcarine cortex. Brain Res. Cogn. Brain Res. 25, 799–809.